Volume 8
Number 46
14 December 2020
Pages 10453–10672

Journal of Materials Chemistry B

Materials for biology and medicine

rsc.li/materials-b

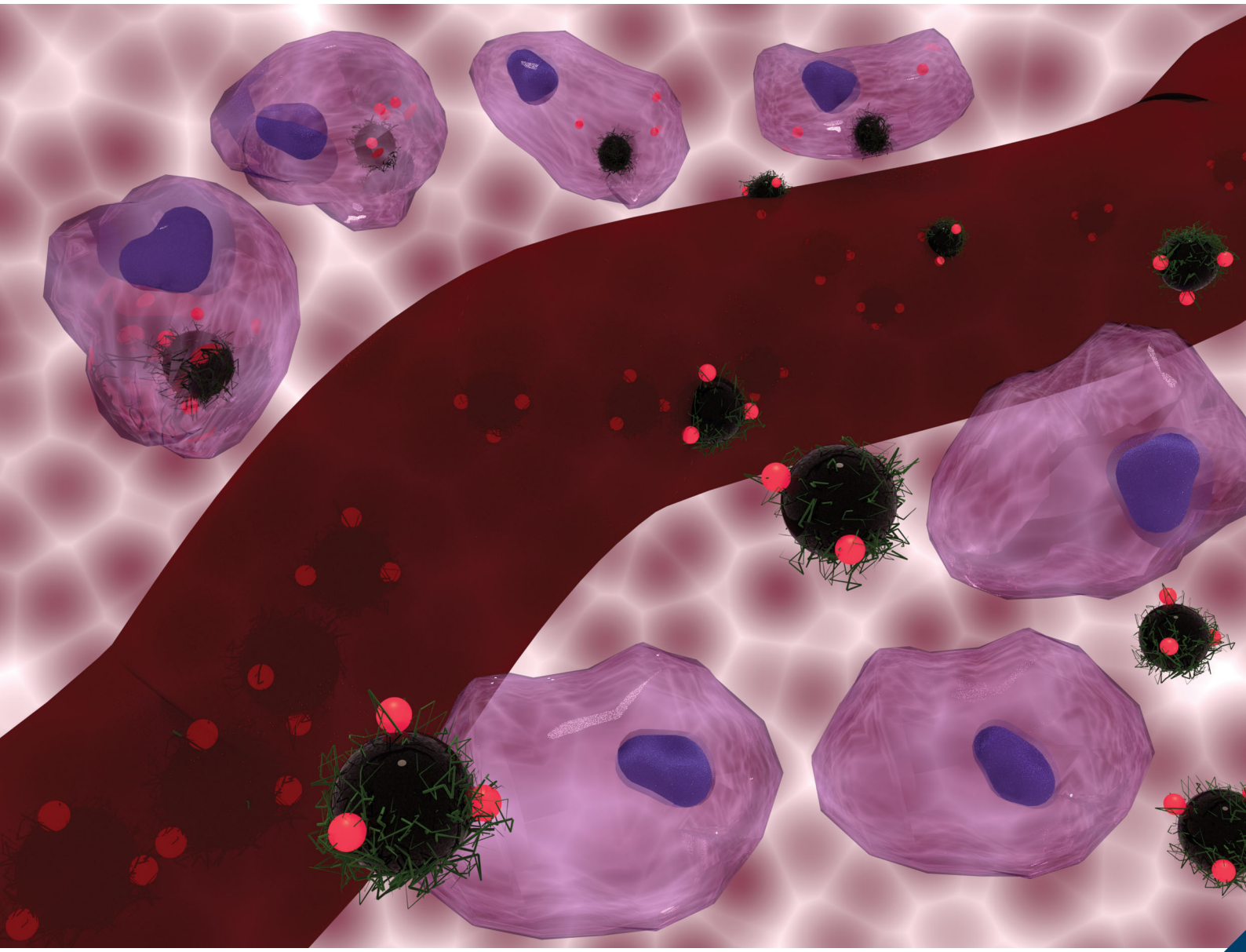

ISSN 2050-750X

ROYAL SOCIETY OF CHEMISTRY

PAPER

Nguyen Thi Kim Thanh *et al.*

In vitro exploration of the synergistic effect of alternating magnetic field mediated thermo–chemotherapy with doxorubicin loaded dual pH- and thermo-responsive magnetic nanocomposite carriers

Journal of Materials Chemistry B

ROYAL SOCIETY OF CHEMISTRY

PAPER

View Article Online
View Journal | View Issue

Cite this: J. Mater. Chem. B, 2020, 8, 10527

In vitro exploration of the synergistic effect of alternating magnetic field mediated thermo–chemotherapy with doxorubicin loaded dual pH- and thermo-responsive magnetic nanocomposite carriers†

Lilin Wang,[ab] Aziliz Hervault,[ab] Paul Southern,[bc] Olivier Sandre,[d] Franck Couillaud[e] and Nguyen Thi Kim Thanh *[ab]

Nanoparticle induced hyperthermia has been considered as a promising approach for cancer treatment for decades. The local heating ability and drug delivery potential highlight a diversified possibility in clinical application, therefore a variety of nanoparticles has been developed accordingly. However, currently, only a few of them are translated into the clinical stage indicating a 'medically underexplored nanoparticles' situation, which encourages their comprehensive biomedical exploration. This study presents a thorough biological evaluation of previous well-developed dual pH- and thermo-responsive magnetic doxorubicin-nanocarriers (MNC–DOX) in multiple cancer cell lines. The cytotoxicity of the nanocomposites has been determined by the MTT assay on primary cell lines. Histology and fluorescence microscopy imaging revealed the efficiency of cellular uptake of nanocarriers in different cell lines. The IC_{50} of MNC–DOX is significantly higher than that of free DOX without an alternating magnetic field (AMF), which implied the potential to lower the systemic cytotoxicity in clinical research. The concurrent thermo–chemotherapy generated by this platform has been successfully achieved under an AMF. Promising effective synergistic results have been demonstrated through *in vitro* study in multi-model cancer cell lines *via* both trypan blue exclusion and bio-luminescence imaging methods. Furthermore, the two most used magnetic hyperthermia modalities, namely intracellular and extracellular treatments, have been compared on the same nanocarriers in all 3 cell lines, which showed that treatment after internalization is not required but preferable. These results lead to the conclusion that this dual responsive nanocarrier has extraordinary potential to serve as a novel broad-spectrum anticancer drug and worth pursuing for potential clinical applications.

Received 15th August 2020,
Accepted 17th October 2020

DOI: 10.1039/d0tb01983f

rsc.li/materials-b

Introduction

Hyperthermia has been considered as a promising therapy for cancer since the last century. Ideally, the tumour compartments with uncontrolled growth cancer cells can be targeted without influence on the function of the surrounding healthy cells. Especially, localized hyperthermia has been demonstrated to eradicate the carcinoma cells *via* multiple ways. On the cellular level, thermal cytotoxicity itself directly kills the cancer cells *via* irreversible cytoplasmic and membrane protein denaturation on the molecular level;[1,2] the absorbed heat provokes numerous apoptosis related cellular pathways, which include cytochrome *c* released mitochondria apoptosis and TNF-related apoptosis-inducing death of receptors DR4, DR5,[3,4] or non-apoptotic cell death such as caspase inflammation enzyme activation.[5] Furthermore, heat shock proteins can also serve as a target motif on the cell membrane for activating and augmenting immune cells against the targeted cells.[6] However, as the clinical results suggest, hyperthermia should be considered as an adjuvant therapy rather than the first choice of treatment at the moment.[7–10] The interest in promoting localized hyperthermia alongside conventional

[a] Biophysics Group, Department of Physics & Astronomy, University College London, Gower Street, London, WC1E 6BT, UK
[b] UCL Healthcare Biomagnetic and Nanomaterials Laboratories, 21 Albemarle Street, London, W1S 4BS, UK. E-mail: ntk.thanh@ucl.ac.uk
[c] Department of Medical Physics and Biomedical Engineering, University College London, Gower Street, London, WC1E 6BT, UK
[d] Laboratoire de Chimie des Polymères Organiques (LCPO), Univ. Bordeaux, CNRS, Bordeaux INP, UMR 5629, 33600 Pessac, France
[e] Molecular Imaging and Innovative Therapies (IMOTION), Univ. Bordeaux, EA7435, Bordeaux, 33000, France

† Electronic supplementary information (ESI) available. See DOI: 10.1039/d0tb01983f

cancer treatment had been absent for a long time until the encouraging synergistic results of the combinational thermo–chemotherapy and thermo–radiotherapy were revealed.[9,11–13]

Generally, the main reason for the failure of both chemotherapy and radiotherapy is attributed to the intricate tumour microenvironment. The advanced stages of solid tumours are characterized by inefficient blood flow, acidic pH and elevated interstitial fluid pressure due to the defective vasculature system caused by cancer angiogenesis. Unlike uniform chromosomal damage caused by the ionizing radiation that can be significantly enhanced by the thermal increased partial O_2 pressure and increased blood flow,[14] the factors and mechanisms involved in the thermo-sensitization of chemotherapy are far more complicated, which impeded its utilization. The different classes of drug interactions with thermal effects undergo diverse mechanisms to suppress cell proliferation.[1] Apart from that, different tumour types, diverse thermo-doses, and heat implementation approaches also contributed to the thermo–chemo sensitisation. One of the proposed mechanisms is the localized intracellular drug concentration being increased by the thermotherapy. The heat exposure in the tumour area can not only elevate drug penetration along with increased epithelial membrane permeability by enlargement of the size of fenestrations between the cells, but also increase the blood perfusion flow rate to reduce the physiological barrier caused by the interstitial fluid pressure.[11,15] However, this benefit could be eliminated when the regional or whole body temperature rises, thus for thermo–chemotherapy, the thermal boosting is critically constrained by the temporal and spatial implementation. Therefore, compared with the conventional hyperthermia approach with radiofrequency electrodes implanted in the tumour, utilization of magnetic nanoparticles (MNPs) for magnetic hyperthermia provides a promising and less invasive solution for concurrent chemotherapy. The high surface to volume ratio of magnetic nanoparticles facilitates the feasibility of drug loading. Once an adequate amount of nanoparticles is accumulated in the tumourigenic region *via* either the enhanced permeability and retention (EPR) effect or external magnetic attraction, the AMF application with high tissue penetration could provide hyperthermia and chemotherapy simultaneously.[16–19]

Hundreds of syntheses of MNPs have been designed since 1957, when the first experimentally reported study by Gilchrist *et al.* in animals (dogs) revealed the feasibility of using MNPs in radiofrequency magnetic hyperthermia.[20] However, in the past six decades, only a few of them have undergone clinical trials and the most successful case is with the Magforce™ company whose treatment NanoTherm® has been approved in June 2010 to go into the high grade glioblastoma brain cancer European market (yet only when combined with conventional radiotherapy), which highlights that MNPs have been highly underexplored.[21,22]

A comprehensive biomedical investigation into MNPs is still needed to make magnetic hyperthermia therapy accessible to the wider population. One of the unsolved issues is to determine which magnetic hyperthermia implementation method is superior:[23] intracellular hyperthermia, where the nanoparticles either have been internalized into the cells or tightly deposited onto the cells, and then the cells are heated directly; or extracellular hyperthermia, where the thermal damages are produced through extracellular matrix (ECM) temperature elevation or ECM mechanical disruption.[24] The proponents of intracellular hyperthermia demonstrated that it could provide a destructive effect despite the absence of macroscopic temperature increases,[25–29] as obtained with intra-tumour injection and the extracellular approach. However, the reported effects varied in the literature. Besides, compared with extracellular strategies, the achievable thermal doses of intracellular hyperthermia are restricted by the insufficient internalization of nanoparticles.[30,31] This issue becomes more complicated when introducing other parameters into the system, such as different chemotherapy drugs and nanoparticle compositions. To date, there have not been many investigations on how intracellular and extracellular magnetic hyperthermia could influence the chemosensitisation effect, particularly with the same type of nanoparticles.

This study presents, for the first time, (i) a comprehensive biological evaluation of our previously well-developed dual pH- and thermo-responsive polymer-coated magnetic doxorubicin-nanocarrier (MNC–DOX) and (ii) multidirectional assessments on the thermally provoked synergistic effects of intracellular/extracellular hyperthermia with the same type of DOX loaded magnetic nanocarrier in multi-model cancer cell lines. The magnetic iron oxide cores were synthesized by the microwave method and conjugated with DOX *via* pH-cleavable imine bonds by a thermo-responsive copolymer. Chemical and physical characterisation and the *ex vivo* drug release pattern of this smart nanocarrier have been previously described by some of us.[32] In the present study, the biocompatibility of the nanocarrier is demonstrated in a primary immortalized murine fibroblast cell line, which is recommended by the ISO10993-1:2009 procedure to assess the biocompatibility of medical devices.[33] Then the cellular uptakes of MNCs in both human breast carcinoma (MCF-7) and glioblastoma (U-87) cell lines have been visualized by histology and fluorescence microscopy at different time points and quantitated *via* Superconducting Quantum Interference Device (SQUID) magnetometry. The half maximal inhibitory concentration (IC_{50}) values of MNC–DOX in all cell lines have been calculated and used to guide the loading during the following combination therapy. In order to acquire comprehensive results, three different cancer cell lines have been investigated: MCF-7 (human breast carcinoma), U-87 (human glioblastoma) and RM1-CMV-LucF (bioluminescent murine prostate cancer cells): for each cell line, approx. the same amount of internalized nanoparticles that has been calculated was loaded onto the cells just before hyperthermia (thus without uptake) in the ''direct treatment'' group, which was used to compare with the ''internalized'' group. Furthermore, the temperature influence on magnetic thermo–chemotherapy has also been analysed by varying different amounts of nanoparticles in the direct/extracellular heating experiment.

Results and discussion

Synthesis of the thermal and pH-sensitive nanocarriers

Briefly, TEM images indicated that, after their synthesis, the bare spherical iron oxide cores had an average size of 13.3 ± 2.2 nm. Their saturation magnetization at 300 K was 70 emu g^{-1}. The successful conjugation of the MNCs, which contained 8.1% of the P(DEGMA-*co*-PEGMA-*b*[TMSPMA-*co*-VBA]) copolymer according to thermogravimetric analysis, has been confirmed by Fourier transform infrared spectroscopy. This copolymer was designed to have a thermosensitive block of diethylene glycol methacrylate and PEG methacrylate with a transition above physiological temperature. The second block possesses units with trimethoxy silane groups for grafting onto the iron oxide surface by the sol–gel reaction and vinylbenzaldehyde comonomer for conjugation to the DOX amine group into a pH-sensitive imide bond.[30] With the help of this hydrophilic polymer coating, the hydrodynamic size of the nanocarrier as measured by dynamic light scattering (DLS) in aqueous media decreased from 194 nm to 120 nm.[30]

Cellular biocompatibility and uptake of MNCs

In this work, the name "MNCs" refers to the P(DEGMA-*co*-PEGMA-*b*[TMSPMA-*co*-VBA]) polymer coated magnetic NPs. In order to apply these nanocarriers in medical applications, crucial factors such as biocompatibility and cellular uptake have been evaluated in multiple cancer cell lines. Nanoparticles with good biocompatibility are investigated to check whether they would induce any degree of toxicity, carcinogenicity or immunogenic response to the biological system.[34] Normally the physical and chemical properties of nanoparticles such as their size, shape, structure, hydrophilicity, hydrophobicity and charge determine the cytotoxicity, but in a biological system the surface coating plays a vital role in the biocompatibility.[35,36] In our system, the magnetic core was composed of a FDA approved material, magnetite, with designed physical properties to be bio-friendly; the thermal and pH sensitive hydrophilic coating contained widely used PEG side chains to prolong the systemic circulation time and prevent aggregation.[37] Thus, the biocompatibility has been assured through this preliminary assay, as expected (Fig. 1).

Doxorubicin, being a widely used chemotoxic drug in cancer treatment, was used in order to evaluate whether our MNC–DOX conjugated system had the potential to benefit patients with different types of cancer. The performances of this system were established for the human glioblastoma U-87 cell line and human breast carcinoma MCF-7 cell line in parallel.

Therefore, the cellular uptake ability of the nanocarriers in both these cell lines were visualized *via* histology staining. After incubation with the MNCs ranging from 0.1 mg mL^{-1} to 1.0 mg mL^{-1} after 4 h or 24 h, the MCF-7 breast cancer cell line and the U-87 glioblastoma cell line were counterstained with nuclear red dye, once the iron oxide nanoparticles were stained with Prussian blue (Fig. 2). In both cell lines, the presence of Prussian blue staining suggested that the MNCs not only got internalized inside the cells, but the uptake also

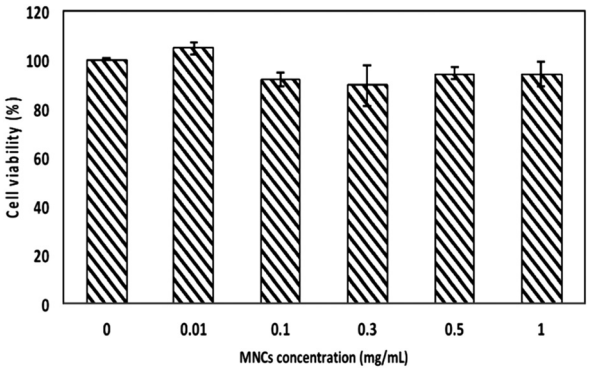

Fig. 1 Biocompatibility study by MTT assay on L929 murine fibroblast cells with increasing concentration of MNCs.

clearly depends on both the nanoparticle concentration and the exposure time. The U-87 cells appeared to obtain more MNCs as compared to the MCF-7 cells at high concentration and incubation time. This result is consistent with other studies in that the nanoparticle uptake capability varies among different kinds of cells and tissues,[38,39] *e.g.* 400 pg iron oxide per cell,[28] the uptake by U-87 cells being even higher, up to 800 pg iron oxide per cell for certain PEGylated multicore MNCs.[40] However, these 2D images are produced by light microscopy, which not only cannot distinguish the internalized MNCs from those that have been only deposited onto the cell membrane, but also cannot quantify these nanoparticles. Meanwhile, a high cellular capture of nanoparticles, be they internalized or tightly deposited, directly corresponds to a higher therapeutic efficiency. Thus, a precise method to quantify the MNCs that have been captured by each cell line is necessary for the following comparison of the therapeutic conducting approaches. Elemental analysis by ICP-MS is a good technique

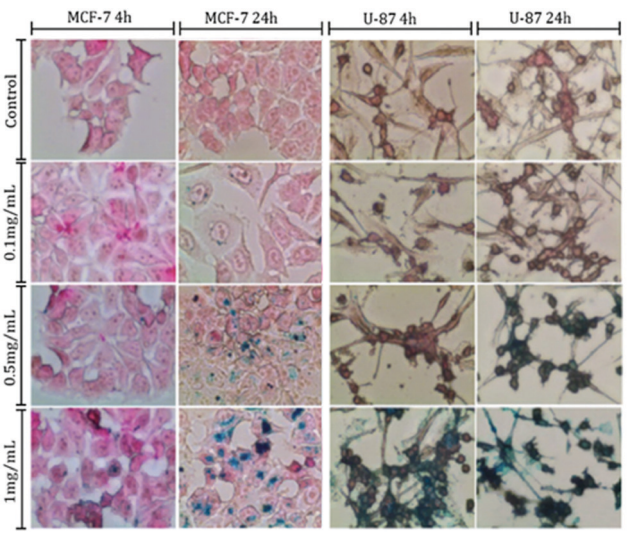

Fig. 2 Microscope images of human glioblastoma U-87 cells and human breast adenocarcinoma MCF-7 loaded with MNCs after 4 h and 24 h of incubation with a solution containing different concentrations of MNCs. Cells were counterstained with Prussian blue and nuclear fast red dyes.

Table 1 MNC uptake quantification of Fe_3O_4 in pg per cell for human glioblastoma U-87 cells and human breast adenocarcinoma MCF-7 after incubation for 4 h and 24 h at different concentrations of MNC solution

		MNC concentration (mg mL^{-1})				
Cell line	Time (h)	0.01	0.05	0.10	0.50	1.00
MCF-7	4	—	—	1	3	6
	24	—	—	2	5	13
U-87	4	—	2	7	15	32
	24	2	6	12	55	125

to quantify the internalized Fe content. However, it cannot distinguish between the endogenous iron cations that may already be there in the cell and the incubated nanoparticles. Superconducting quantum interference device (SQUID) magnetometry is the only technique that characterizes exclusively the magnetic iron oxide nanoparticles in the biological system. Thus, the magnetic measurements of cells loaded with MNCs have been carried out by SQUID magnetometer measurements for quantification (Table 1). Comparison of the nanoparticle cellular internalization *via* both techniques has confirmed that the cellular uptake of U-87 cells was higher than that of MCF-7 cells.

Apart from the MNC internalization, the intracellular localization of DOX is also critical in designing nanocarrier anticancer activity, as the therapeutic efficiency of this system is also determined by the DOX inhibition of the topoisomerase enzyme in the nucleus through binding to the tumour cell chromosome.[41,42] Hence, the internalization of DOX, exhibiting an intrinsic red fluorescence, in U-87 and MCF-7 cells after incubation with either free DOX or MNC–DOX has been assessed by fluorescence microscopy (Fig. 3).

Generally, the results revealed that the overall DOX accumulation of MNC–DOX for short term incubation *in vitro* was efficient for both cell lines but seems lower than for the free drug, while the patient's ultimate clinical outcome should benefit from the endocytic drug uptake and thermo-acidic dual controlled release pattern of MNC–DOX. The intracellular signals of free and encapsulated forms of DOX in both cell lines were detectable even just after 3 h of incubation, and the signal intensities were amplified with increased incubation time. However, comparison between the free DOX and MNC–DOX at each time point within the same cell lines indicated that the signal of free DOX was significantly stronger than with the nanoparticle loaded system, which implies that the free DOX has quicker and higher cellular accumulation in *in vitro* cultures. Besides, the DOX intensity from MCF-7 cells was lower than that from U87 implying that the U87 cell lines can engulf more DOX–MNCs, which is comparable to the observed cellular uptake of this nanocarrier as demonstrated by previous dye staining and SQUID magnetic measurements.

Furthermore, merging the DOX signal with blue emitting nucleus indicator DRAQ5 exposed the detailed intracellular localisation of DOX *in vitro*. It showed that the free DOX was rapidly accumulated in the cell nucleus whereas our nanoparticle conjugated DOX was mainly captured in the cytoplasm

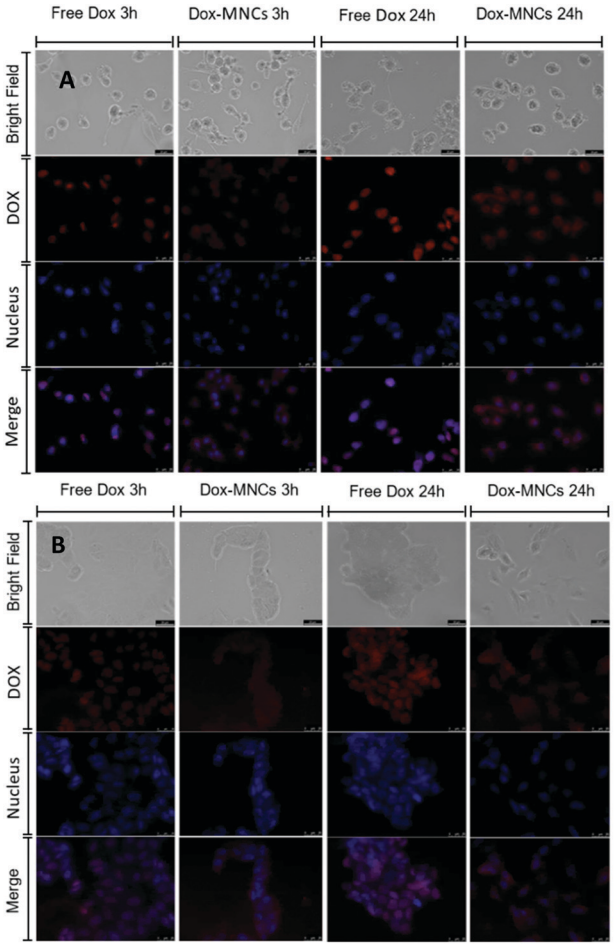

Fig. 3 Fluorescence images of U87 cells (A) and MCF-7 cells (B) after 3 h and 24 h of incubation with either free DOX or DOX–MNCs. Cell nuclei were counterstained with blue dye DRAQ5. Scale bar: 20 μm.

even after 24 h incubation. This evidence is not only consistent with the other published nanostructure based DOX delivery patterns, by which the nano-structure based carriers are predominantly taken up by the slower endocytosis pathway into endosomes rather than by the rapid passive diffusion that free DOX tends to go through; but also these experimental results verified that our system is an efficient drug delivery system as that demonstrated in our previous *ex vitro* cumulative drug release profiles.[43–46] Only a small proportion of DOX was released from the endocytic organelle due to the gradual hydrolysis of the Schiff base linkage bond between the drug and polymer, most of the drug still remaining in the cytoplasm within the stable MNC carrier until the temperature stimulus has been applied.[32] Normally, the particles between 10 to 100 nm can internalize into the cells easily and quickly with either clathrin-mediated endocytosis or caveolae-mediated endocytosis.[47,48] However, studies revealed that particles from hundreds of nanometers up to 5 μm in size can enter cells through macropinocytosis, characterized by ruffles that formed on the cell membrane that protrude to engulf the larger particles.[49] In our study, the nanocarriers have a hydrodynamic size of 120 nm with a PDI of 0.16.[30] This means that the

suspensions have a broad range of size distribution, which contains particles both under the 100 nm threshold and above it. Thus, these nanocarriers may enter the cells under different pathways depending on their size.

Therefore, our drug delivery system on the one hand has the potential to diminish the extracellular free DOX induced acute whole-body cytotoxicity, and on the other hand it may circumvent the multidrug resistance associated with transporter provoked DOX effluxion *via* the endocytic uptake pathway, thus compared to free DOX it is more suitable for clinical application.[50,51] The dual responsive magnetic nanocarriers are biocompatible and are taken up efficiently by two different cancer cell lines yet avoiding passive diffusion by efflux pumps through the cell outer membrane.

Cytotoxicity of DOX *vs.* MNC–DOX in the absence of AMF

Cell cytotoxicity induced by different concentrations of DOX at three exposed durations (24 h, 48 h and 72 h) has been examined and compared between DOX–MNCs and the free DOX through MTT cell viability assay for glioblastoma and breast carcinoma cell lines. The IC_{50} values (Table 2) for each condition have been determined and designated as the loading dose for the formulation in the following combination treatment, consequently. For both the cell lines, DOX concentration and incubation time dependent cytotoxicity effects were obtained for different exposure times (Fig. 4). Comparison within the same cell line shows that the free DOX is much more cytotoxic than the DOX–MNCs. The IC_{50} values for the encapsulated DOX group are nearly 10 times higher than for the free ones on average. Especially for the breast cancer cell lines, the IC_{50} is even higher than 10 μg mL^{-1}. This lower cytotoxicity effect of the DOX–MNCs verified the previous results on the DOX and MNC uptakes. As DOX molecules conjugated to the MNCs go through an endocytosis pathway that needs longer uptake time than the free DOX and without AMF stimulation, the majority of the drug still remained inside the endosomes or lysosomes with the nanocarriers, subsequently inducing less cytotoxicity as a result of less drug exposure to the nucleus.

AMF treatment of cancer cell loaded DOX–MNCs

Either a high concentration of a chemotherapeutic drug or a high temperature is enough to kill cancer cells. For the anticancer thermo–chemotherapy combination treatment, the evaluation of the synergistic effect, particularly at low doses, is necessary for assessing therapeutic efficiency. For this purpose, our experiments have been performed at low concentration of DOX close to the IC_{50} value, *i.e.* 0.15 μg mL^{-1} for the U87 cell lines and 5.25 μg mL^{-1} for MCF-7 cell lines.

Table 2 IC_{50} values of human glioblastoma U-87 cells and human breast adenocarcinoma MCF-7 cell lines after exposure with free DOX or DOX–MNCs for 24 h, 48 h and 72 h

	Cell line	Time (h)	24	48	72
IC_{50} (μg mL^{-1})	U-87	Free DOX	0.13	0.06	0.04
		DOX–MNCs	0.90	0.12	0.50
	MCF-7	Free DOX	0.95	0.29	0.16
		DOX–MNCs	>10	7.91	>10

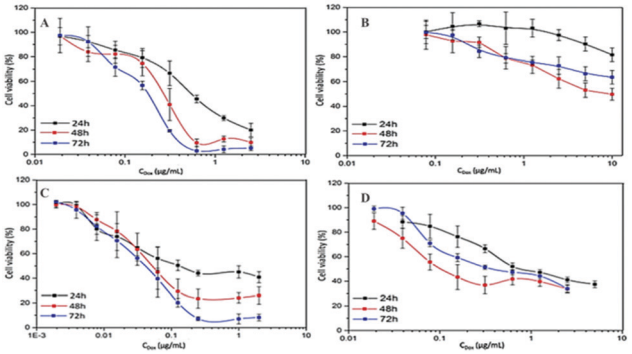

Fig. 4 Dose response curves of human breast adenocarcinoma MCF-7 (A) and (B), human glioblastoma U-87 cells (C) and (D) and incubated with DOX concentrations of either free DOX (A and C) or DOX–MNCs (B and D), all for 24 h, 48 h and 72 h.

As mentioned previously, conclusions about the additive or synergistic effects of combined thermo–chemotherapy from numerous publications suggested that different implementation approaches of hyperthermia might contribute to the overall therapeutic effect.[52] The extracellular hyperthermia and intracellular hyperthermia are the two most common approaches for magnetic fluid induced hyperthermia in the literature, but they introduce the heat from totally different cellular locations.[26,53–55] In this study, extracellular heating involves subjecting the cells directly to hyperthermia treatment immediately after mixing with the nanoparticles, thus applying heat originating only from the surrounding medium. The intracellular treatment was performed after 24 h internalization of 1 mg mL^{-1} suspension of nanoparticles with cells and subsequent washing of the extracellular nanoparticles. In this case, the heat is only generated by the nanoparticles internalized in endocytic components. Consequently, comparison of the synergistic effect between the two treatments in cancer cell lines could determine whether a heat treatment being released from the inside of the tumour cells or from the surrounding medium is more efficient for thermo–chemotherapy.

The internalized hyperthermia treatment has been performed under an AMF with a frequency of 950 kHz and a field amplitude of 10.5 kA m^{-1} for 1 h. The cell viability at different time points after treatment was assayed with the trypan blue exclusion method. Previous publications have already verified that the AMF implementation does not affect cell viability.[55] In order to eliminate unexpected variation, the cell AMF positive controls have been evaluated at 48 h time point in this study. The one-hour real-time heating curves indicate that the local temperatures of the glioblastoma cell line U87 suspensions were mainly retained at 39.2 °C, while the MCF7 cell suspensions stabilize at a lower temperature of 37.7 °C, due to the lower cellular uptake (see Suppl. 1, ESI†). For both cell lines, the treatment procedure was below the normal mild hyperthermia temperature of 42 °C. Accordingly, the cell viability in the hyperthermia alone group only showed 20–30% reduction

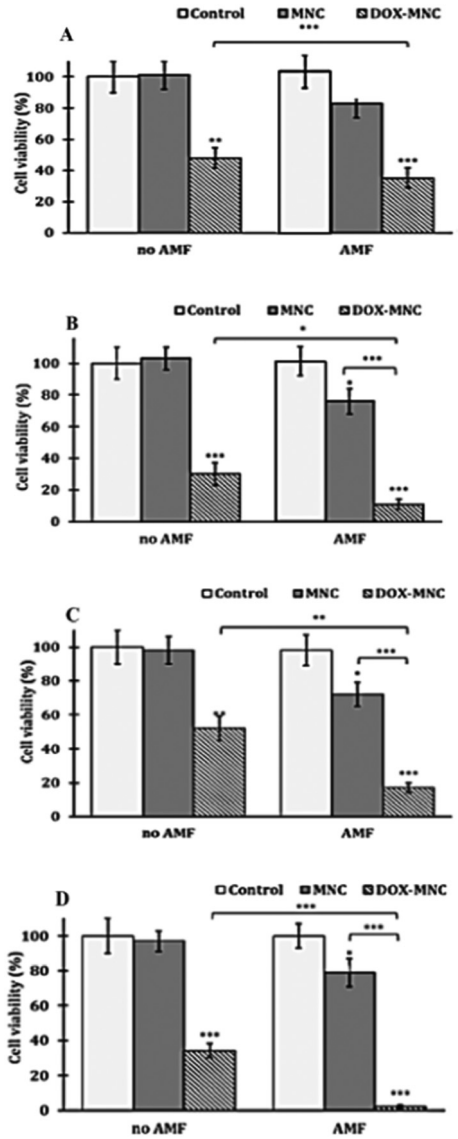

Fig. 5 24 h (A and C) and 48 h (B and D) post treatment cell viabilities of internalized nanoparticle hyperthermia for MCF-7 cells (A and B) and U-87 (C and D) after exposing with or without an AMF (1 h at f = 950 kHz and H = 10.5 kA m^{-1}) with media alone (control cells), MNCs or DOX–MNCs. The asterisks refer to significant levels compared to the corresponding control experiment or the combined therapy; $p < 0.05$ (*), $p < 0.01$ (**) and $p < 0.001$ (***).

(Fig. 5). Cellular viability decrease within 48 h after one-shot of hyperthermia is consistent with the heat induced apoptosis pattern.[2,56] Notably, the U-87's cell viability has an increasing trend from 72% to 79% within two days post-treatment incubation, which suggests that cells started recovering from insufficient thermal exposure. The ability of cancer recovery from underestimated dose and even generating further thermal resistance also indicates the ongoing challenge in using hyperthermia alone in cancer treatment, as the complex tumour architecture and lack of reliable in site real-time temperature measurement made it nearly impossible to conduct a uniform and controlled heating dose among all the cancer cells.[55] Hence, a successful combinational treatment of hyperthermia and thermotherapy provides an important and significant improvement to the current therapeutic strategy.

The result of our internalized combination treatment showed a statistically significant tumour cell suspension compared to the chemo treatment alone. The 48 h results are prominently promising as the cell viability for U87 and MCF7 has been remarkably reduced to 4% and 11%, respectively. The combinational effectiveness has further been numerically assessed by Valeriote's method (Table 3).[57] Surprisingly, even at temperatures under the mild hyperthermia range, both cell lines have presented a synergistic effect of thermo–chemotherapy compared to thermo- or chemotherapy alone.

Direct treatment of cancer cells with DOX–MNCs

The direct treatment of cells has been performed by an identical hyperthermia protocol with the same dose of DOX but different amounts of MNCs. The same quantity of nanoparticles that got internalized by the cells after 24 h were incubated with the 1 mg mL^{-1} of nanoparticles, which is 75 μg per well that has been used to compare with previous intracellular thermo–chemotherapy (Suppl. 2, ESI†). Besides, direct treatment with 200 μg and 300 μg of MNCs was also used to assess whether the higher temperature reached affects the effectiveness of the thermo–chemotherapy treatment.

The real-time heating curve of the cell suspensions at different MNC concentrations is shown in Suppl. 2 (ESI†). The temperature of internalization equivalent to the direct treatment group, 75 μg mL^{-1}, has reached a similar temperature to previous internalized magnetic hyperthermia treatment, 40 °C. The 200 μg mL^{-1} and 300 μg mL^{-1} groups approached mild hyperthermia temperatures of 42 °C and 44 °C, respectively. The cell viability measured at 24 and 48 h after direct treatment for both hyperthermia alone and combination therapy exhibited a dramatic decreasing trend with regard to the increased thermal dose for both cell lines (Fig. 6): thermosensitivity is thus similar in both cell lines. It is worth mentioning that an impressive cell elimination by the increased thermal does has been obtained in the hyperthermia alone group when the temperature reached 44 °C. The cell viability has dropped to 24% after 48 h post hyperthermia in MCF-7 cell lines and 26% in U-87 cell lines. This also indicates that an even higher temperature is required for hyperthermia alone. At each temperature, the combinational treatment demonstrated clear statistically significant superiority over individual treatment. The most potent combination result has been detected with the

Table 3 Evaluation of the combined effect of the thermo (A)–chemo (B) therapy treatment on the cell survival rate after nanoparticle internalization for both MCF-7 and U-87 cell lines according to Valeriote's formula

	Time (h)	(AXB)/100 (%)	(A + B) (%)	Effect
MCF-7	24	40	35	Synergistic
	48	23	11	Synergistic
U-87	24	37	17	Synergistic
	48	27	2	Synergistic

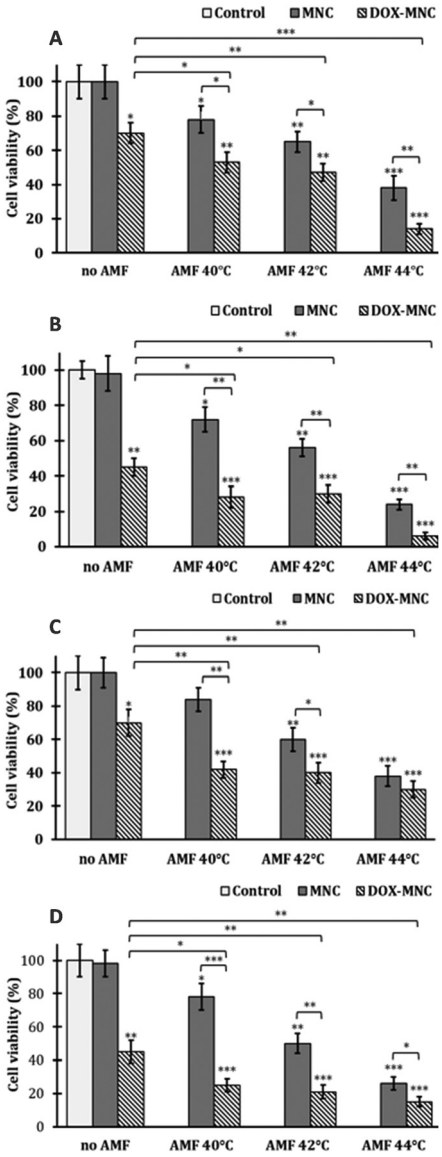

Fig. 6 24 h (A and C) and 48 h (B and D) post treatment cell viabilities of direct hyperthermia for MCF-7 (A and B) cells and U-87 (C and D) following direct treatment with or without a 1 h exposure to an AMF (f = 950 kHz and H = 10.5 kA m^{-1}) with media control or contain MNCs or DOX–MNCs. The asterisks refer to significant levels compared to the corresponding control experiment or the combined therapy; $p < 0.05$ (*), $p < 0.01$ (**) and $p < 0.001$ (***).

highest thermo-induced temperature, 44 °C as expected, at which the cell viability has decreased to 6% in the MCF7 cell line and 15% in the U-87 cell line. The synergistic efficiency that has been assessed *via* Valeriote's method is shown in Table 4.[57] Apart from the sub-additive effect of thermo–chemotherapy that was reported at 44 °C in U-87 cells and 42 °C in MCF-7 cells, the direct treatment of cancer cells with our drug delivery system has shown synergistic effects under all the other conditions. Furthermore, the maximum synergistic ratio of combination treatment has been observed at 40 °C in U-87 cell lines and 44 °C in MCF-7 cell lines, and the synergistic effect in U-87 cell lines was diminished by increasing the magnetic hyperthermia

Table 4 Evaluation of the combined effects on the cell survival rate of the direct thermo–chemotherapy treatment at different hyperthermia temperatures for MCF-7 and U-87 cell lines according to Valeriote's formula

		Time (h)	(AXB)/100 (%)	(A + B) (%)	Effect
MCF-7	40 °C	24	55	53	Synergistic
		48	32	28	Synergistic
	42 °C	24	46	47	Sub-additive
		48	25	30	Sub-additive
	44 °C	24	27	14	Synergistic
		48	11	6	Synergistic
		Time (h)	(AXB)/100 (%)	(A + B) (%)	Effect
U-87	40 °C	24	59	42	Synergistic
		48	35	25	Synergistic
	42 °C	24	42	40	Synergistic
		48	23	21	Synergistic
	44 °C	24	27	32	Sub-additive
		48	12	15	Sub-additive

temperature. The higher synergistic ratio at low temperature in a specific cell line is of particular importance: if only a low hyperthermia temperature is needed for the treatment, the quantity of nanoparticles necessary for the treatment will remain low and achievable in the clinic, potentially achievable by intravenous injection instead of intra-tumoural as in the MagneTherm® protocol.

These results imply that different thermal doses could lead to distinctive thermo–chemosensitisation effects in particular cell lines, which emphasizes the importance of an appropriate thermal dose in designating direct thermo–chemotherapy for individual cell lines. The mechanisms behind this phenomenon may be contributed to by the different behaviours driven from different cell lines and non-linear thermal induced cellular uptake of chemodrugs.[58] In the direct treatment, there was not enough time for nanoparticles to be taken up by the cells, which means unlike internalized modality most of the antineoplastic drugs were only released by heating outside of the cells.

Although the increased cell membrane permeability associated with promoting drug accumulation into tumour cells by raising temperature has been proved,[59] some publications demonstrated, for DOX, a prominent increase of intracellular accumulation reported with 40 °C hyperthermia which was not observed at 43 °C, *in vivo*.[60,61] This result corroborates our finding of sub-additive effects observed at 44 °C in the case of U-87 cells. Direct treatment (*i.e.* extracellular) of cancer cells with DOX–MNCs shows either a synergistic or sub-additive effect.

Synergistic effect of DOX–MNCs on the RM1-CMV-LucF cells

The promising synergistic results of DOX–MNC induced thermo–chemotherapy on both MCF-7 and U-87 human cell lines have revealed the potential to apply this system to other cell lines. However, the thermosensitisation differences between two cell lines also highlight the importance of elaborative analysis of particular cell lines before application. Moreover, the previous evaluation was based on the trypan blue dye exclusion assay, which may underestimate the therapeutic efficiency by excluding the cells that undergo an early disintegration. Thus, the combinational treatment of our system in

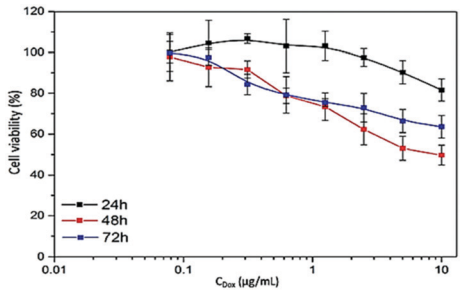

Fig. 7 Dose–response curves of RM1-CMV-LucF cells incubated with DOX–MNCs in the series of dilutions according to DOX concentration for 24 h and 48 h incubation.

genetically modified murine prostate cancer cell line RM1-CMV-LucF has been tested *via* a bioluminescence imaging (BLI) assay.[62] The cytotoxicity effects of DOX–MNC alone and combination of intracellular and extracellular hyperthermia treatments were examined by monitoring their luciferase expression, which is correlated with cell metabolic activity, through the BLI method.

The dose–response curve of the cytotoxicity of DOX–MNCs after 24 h and 48 h incubation is illustrated in Fig. 7. This shows an increasing cytotoxicity with higher DOX concentration or longer incubation time. The IC_{50} values after 24 h and 48 h of incubation were found to be equivalent to a DOX concentration of 2.12 μg mL^{-1} and 0.16 μg mL^{-1}, respectively. According to this, a low DOX concentration of 0.18 μg mL^{-1} in the subsequent experiments has been used to analyse the synergistic effect. As the preliminary tests have shown that 42 °C was more efficient for the combined therapy than hyperthermia at 40 °C or 44 °C for this specific cell line, the hyperthermia temperatures of 42 °C and 43 °C were studied in the direct treatment. During the 30 min hyperthermia under the AMF with f = 217 kHz and H = 20 kA m^{-1}, the temperature has been adjusted and maintained by tuning the field amplitude H along the AMF application. The outcome of either intracellular hyperthermia or extracellular hyperthermia exhibited a similar decreasing pattern with previous MCF-7 and U-87 cell lines (Fig. 8). The cytotoxic effect of the combinatorial treatment achieved with a developed nanodrug delivery system was found to be statistically superior to either hyperthermia or chemotherapy applied separately. This satisfactory synergistic effect of the thermo–chemotherapy for both hyperthermia methods has been evaluated numerically by Valeriote's formula in Table 5. Notably, the cell viability of hyperthermia treatment alone after internalization reached as low as 65%, which is a drastically higher toxic effect than 89% at 42 °C and 71% at 43 °C in direct treatment. This noticeable viability reduction by internal hyperthermia has not been observed in the other two cell lines, which suggests that RM1-CMV-LucF cell lines may be more sensitive to the heat released from intracellular nanoparticles.

Comparison between the intracellular hyperthermia and extracellular hyperthermia in combination therapy in all three cell lines has highlighted that the method of conducting magnetic hyperthermia greatly influences the combination therapy results. No matter whether a cell line has internalized

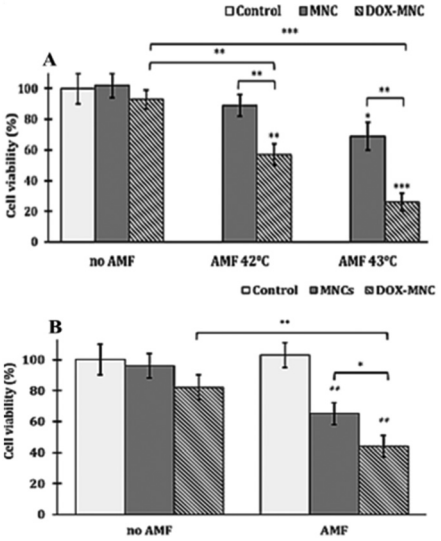

Fig. 8 Cell viabilities of RM1-CMV-LucF cells 24 h following either (A) direct treatment or (B) treatment after internalization. The asterisks refer to significant levels compared to the corresponding control experiment or the combined therapy; $p < 0.05$ (*), $p < 0.01$ (**) and $p < 0.001$ (***).

Table 5 Evaluation of the combined effects of the thermo–chemotherapy treatment after nanoparticle internalization or direct thermo–chemotherapy treatment at different hyperthermia temperatures for the RM1-CMV-LucF cell line according to Valeriote's formula. In the case of intracellular hyperthermia, the temperature did not increase under AMF application (*i.e.* it remained 37 °C)

		(AXB)/100 (%)	(A + B) (%)	Effect
Intracellular treatment	—	53	44	Synergistic
Extracellular treatment	42 °C	83	59	Synergistic
	43 °C	64	27	Synergistic

the desired nanoparticles in a high amount, such as the U-87 cells, or not, like MCF-7 cell lines, the intracellular hyperthermia induced a better thermo–chemotherapy synergistic result than the extracellular treatment method (Tables 3–5). Remarkably, in the high nanoparticle uptake U-87 cell line, the cell viabilities for the combined therapy in the intracellular heating group reached values as low as 17% and 2%, 24 h and 48 h after the treatment, respectively. The results were not only lower than the equilibrated direct therapeutic group, 40% and 25%, but also, more pronounced than the best outcomes achieved in the direct hyperthermia group, 32% and 15%. Although a promising thermo-chemotherapy result has been accomplished in all cells with both hypothermia methods, the finding demonstrates that it is more effective therapy if tumour cells internalise the nanoparticles.

Experimental

Materials

Materials for nanocarrier synthesis. Iron(II) chloride tetrahydrate, iron(III) chloride hexahydrate, sodium carbonate,

hydrochloric acid, poly(ethylene glycol) methyl ether methacrylate, di(ethylene glycol) methyl ether methacrylate, 3-(trimethoxysilyl) propyl methacrylate, 3-vinylbenzaldehyde, 4,4-azobis(4-cyanovaleric acid), 4-cyano-4-(phenylcarbonothioylthio)-pentanoic acid, chloroform-d NMR solvent, triethylamine, acetonitrile, toluene, and petroleum ether were purchased from Sigma-Aldrich, UK. Tetrahydrofuran was provided by Wako chemicals, UK.

Materials for biological experiments. 0.4% Trypan blue solution, dimethyl sulfoxide (DMSO, purity $\geq$99.9%), hydrochloric acid (HCl, 37 wt%), hexacyanoferrate trihydrate ($K_4Fe(CN)_6{\cdot}3H_2O$), nuclear fast red (0.1%, w/v), accutase solution and minimum essential cell growth medium eagle (MEM) were purchased from Sigma-Aldrich, UK. 3-(4,5-Dimethyl-2-thiazolyl)-2,5-diphenyl-2*H*-tetrazolium bromide (thiazolyl blue tetrazolium bromide MTT, 98%) was obtained from Alfa Aesar, UK. Ethanol (100%) was obtained from Hayman, UK. The other chemicals and media were acquired from Gibco Thermo Fisher scientific, UK. All sterile reagents were used as purchased without any further modification; the rest were sterile filtered to avoid any contamination in the biological procedure.

Synthesis of a doxorubicin loaded magnetic nanocarrier

The superparamagnetic nanoparticle cores in this nanocarrier were first synthesized *via* a modified co-precipitation method with the aid of a microwave reactor (CEM Discover SP).[30,56] Then the P(DEGMA-*co*-PEGMA-*b*-[TMSPMA-*co*-VBA]) polymer, which was synthesized by adjusted reversible addition–fragmentation chain transfer (RAFT) polymerization, was grafted onto the nanoparticle surfaces through the silanisation reaction between the hydroxyl groups of the bare magnetic nanoparticle and the trimethoxysilane groups of the polymer.[63] Finally, the doxorubicin was conjugated to the MNCs through the formation of pH-cleavable Schiff base bonds.[30] Full characterisation has been performed to control the quality of the nanocarriers before their use in biological experiments.

Cell culture

The U87-MG glioblastoma cell line, mouse fibroblast cell line L929 and genetic modified Luciferase firefly (LucF) expressed murine prostate carcinoma cell line RM1-CMV-LucF were cultured in Dulbecco's modified Eagle's medium (DMEM), while theMCF7 breast cancer cell line was cultured in MEM. All complete media were supplemented with 10% foetal bovine serum (FBS), 1% penicillin/streptomycin and 1% L-glutaMAX. The cells were cultured at 37 °C under 5% CO_2 in humidity stable incubators. They were detached at approximately 80–90% confluence by trypsinization for the further experiments.

Intracellular internalization imaging

In order to identify the intracellular internalization of MNCs, the Prussian blue (PB) staining assay was used to visualize the iron oxide core. Fluorescence microscopy was employed to track the DOX in cells from its red emission.

Prussian blue histology staining. Prior to both visualizations, MCF-7 and U87 cells were grown on coverslips at a density of 5.0×10^4 cells per well inside 24 well plates for 72 h to reach confluence. Then for the Prussian blue histology staining, the cell culture was substituted by MNC suspension medium with different concentrations: 1 mg mL^{-1}, 0.5 mg mL^{-1}, 0.1 mg mL^{-1}, 0.05 mg mL^{-1}, 0.01 mg mL^{-1} and 0.00 mg mL^{-1} for 4 h or 24 h to allow particle internalization. Followed by washing three times with complete medium and twice with Dulbecco's phosphate-buffered saline (DPBS), the cells were fixed with 4% paraformaldehyde for 30 min at room temperature. Afterwards, the cells were stained with freshly prepared Prussian blue solution for 2 min and counterstained with nuclear fast red for another 2 min. Finally, the cells were dehydrated with alcohol and mounted onto microscope glass slides for fluorescence imaging on an inverted optical microscope (DMI600B, Leica, UK).

Fluorescence microscopy. After cell confluence, the culture medium was replaced by 1 mL of medium containing either DOX solution or DOX–MNCs with an equivalent amount of 4 μg DOX for 3 h or 24 h. Then the free DOX or nanocarriers were fully removed by washing four times with medium and twice with DPBS. After 30 min 4% paraformaldehyde fixation, the cell was rinsed twice again with DPBS before it was stained with 5 μM nuclear dye, DRAQ5, for 15 min in the dark. The coverslips were rinsed with Milli-Q water and mounted in a slide using Fluor Preserve mounting medium before observation with a microscope (DMI600B, Leica, UK). An excitation wavelength of 488 nm was used for both DOX and DRAQ5. The fluorescence emissions of these two were observed using rhodamine (N3 ET, 600/40 bandpass filter, Leica) and far-red (Y5 ET, 700/75 bandpass filter, Leica) filter sets, respectively. Images were captured using LAS X software.

Quantification of intracellular iron content

The SQUID magnetometer (PPMS, Quantum Device™) was used to quantify the MNC content in MCF7 and U87 cell lines. The cells were cultured in 12 well plates at 1.0×10^5 cells per well seeding density for 72 h, and then treated with different concentrations of MNC containing medium (*i.e.* 1 mg mL^{-1}, 0.5 mg mL^{-1}, 0.1 mg mL^{-1}, 0.05 mg mL^{-1}, 0.01 mg mL^{-1} and 0.00 mg mL^{-1}) for 4 or 24 h to allow the internalization of the MNCs. After gently removing the free nanoparticles by washing three times with medium and twice with DPBS too, the cells were collected by trypsinization and centrifugation. The total cell number was estimated by calculating the cell density of 0.5 mL re-suspending cell pellet medium using a haemocytometer. Then, the cell pellets were collected by centrifugation again and transferred into a powder polycarbonate sample holder for SQUID-VSM. Samples were dried in a low temperature oven at 37 °C overnight before carrying out the magnetic measurements.

Cytotoxicity and cell viability assays

MTT assay. After incubation and treatment, the MTT solution was added to every well to a final concentration of 200 μg mL^{-1} incomplete cell culture medium for 4 h. Then, the MTT containing medium was discarded and a fixed amount of DMSO was added into the wells to dissolve the formazan

crystals. The proportion of viable cells was calculated by absorbance measured on a microplate reader (VersaMax™, Molecular Devices, USA) at 540 nm.

Trypan blue dye exclusion assay. Cells from each treatment group were trypsinized with 0.4 mL trypsin and dispersed in 1 mL of fresh media. 50 μL of cell suspension was stained with an equal amount of sterile-filtered trypan blue and then counted using a haemocytometer. The viability of the treated group was calculated relative to the corresponding control.

Bioluminescence assay. Briefly, at the end of incubation the medium was removed from RM1-CMV-LucF cell cultures before washing with DPBS. D-Luciferin was added at 6×10^{-4} M and the bioluminescence image was captured 5 min later on an IVIS Lumina™ LT (PerkinElmer Inc., USA) and analysed using Living Image® software. The percentage of viable cells for each group was expressed as a percentage of the vehicle control.

Biocompatibility evaluation

L929 cells were plated in 96 well plates at a concentration of 1.0×10^3 cells per well for 72 h. Then 100 μL of medium in each well was replaced by different concentrations of MNC containing medium, from 0 to 1 mg mL^{-1}, and incubated for another 48 h. Finally, the cell viability was calculated by the MTT assay.

Cytotoxicity comparison

In order to evaluate the cytotoxicity difference between free DOX and DOX–MNCs at different exposure times among cell lines and to provide the potency baseline for the following combination treatment assays, the IC_{50} was calculated *via* CompuSyn® software.

The IC_{50} determination for MCF7 and U87 cell lines. Cells were plated in 96 well plates at a concentration of 5.0×10^3 cells per well. After 24 h, different concentrations of medium that contain either free DOX or DOX–MNCs were added into the cells for another 24, 48 or 72 h. High concentration DOX stock was diluted in DMSO. Control wells contained the same amount of DMSO, to normalize the cell cytotoxicity coming from the vehicle. The MTT assay was performed as previously described.

RM1-CMV-LucF cell line. Cells were plated at 2.5×10^4 cells per well in 24 well plates for 48 h before growing in different concentrations of either free DOX or DOX–MNCs containing medium for another 24 h and 48 h. After that, the cell viability was calculated based on the photon counts in the region of interest (ROI) placed on bioluminescence images of each well.

Treatment protocol for thermo–chemotherapy evaluation

In order to evaluate the synergistic effect of magnetic nanoparticles in the combination treatment over hyperthermia itself *in vitro*, both direct and internalized hyperthermia protocols have been conducted for all cell lines. In each set of experiments, the cultured cell has been grouped as follows: control, treated with MNC and DOX–MNC groups. Half of them have gone through AMF induced hyperthermia, and the rest stayed as controls. Hyperthermia groups: control+ (media only, AMF), MNCs+ (media containing MNCs, AMF) and DOX–MNCs+ (media containing DOX–MNCs, AMF). Hyperthermia control groups: control (media only, no AMF), MNCs− (media containing MNCs, no AMF) and DOX–MNCs− (media containing DOX–MNCs, no AMF). The the combination effect was evaluated by Valeriote's method as follows:

- synergistic: $(A + B) < (A) \times (B)/100$
- additive: $(A + B) = (A) \times (B)/100$
- sub-additive: $(A) \times (B)/100 < (A + B) < (A)$ if $(A) < (B)$
- interference: $(A) < (A + B) < (B)$, if $(A) < (B)$
- antagonistic: $(B) < (A + B)$, if $(A) < (B)$.

A and B stand for the cell viability for hyperthermia and chemotherapy respectively.

Intracellular thermo–chemotherapy

MCF7 and U87 cell lines. The seeding density for 12 well plates is 1.5×10^5 cells per well. After 24 h pre-incubation, MNCs or DOX–MNCs at a concentration of 1 mg mL^{-1} of Fe and 0.15 μg mL^{-1} of DOX were added into the cells for 24 h to allow their full internalization. Subsequently the free nanoparticles were washed away and the cells from each group were collected and redisposed in 0.5 mL medium before applying hyperthermia under an AMF H = 10.5 kA m^{-1} and f = 950 kHz for 1 h using a MACH instrument (Resonant Circuits Limited, London, UK). After treatment, the cells were seeded in 12 well plates and their viability was analysed after 24 or 48 h *via* the trypan blue dye exclusion assay.

For RM1-CMV-LucF cell line. 1.0×10^5 cells were grown in 3 mL of medium in every 35 mm culture dish for 48 h before being treated with fresh media or the media that contained 1 mg mL^{-1} of iron containing MNCs or DOX–MNCs. Then the free MNCs and DOX–MNCs were washed away from cells after 24 h internalization. The 3 AMF positive groups were exposed to H = 20.0 kA m^{-1} and f = 217 kHz magnetic field for 30 min using the DM3 instrument (Nanoscale Biomagnetics™, Zaragoza, Spain). The AMF negative groups were subjected to the same protocol without being treated with magnetic hyperthermia. After the 30 min treatment, the cells were incubated for 24 h before measuring the cell viability by the BLI measurement method.

Extracellular thermo–chemotherapy

MCF7 and U87 cell lines. The same protocols as for the after-internalization method was used, except that the nanoparticles for direct heating were added only right before the exposure of the cells to hyperthermia treatment. Briefly, after collecting the cell pellet, 0.5 mL of fresh media or MNC or DOX–MNC containing media were transferred into a vial for hyperthermia treatment. The DOX in all nanocarrier groups was 0.15 μg mL^{-1} that is the same as treatment after the internalization protocol. An iron concentration of 75 μg mL^{-1} was used for the hyperthermia treatment at 40 °C, which was equal to the nanoparticle concentration internalized after exposure of U-87 cells for 24 h with a solution of 1 mg mL^{-1} of MNCs. Concentrations of 200 μg mL^{-1} and 300 μg mL^{-1} were used for the hyperthermia treatment at 42 °C and 44 °C, respectively. After

this, identical treatments and analysis procedures were used as mentioned in the internalization hyperthermia protocol.

Test for the RM1-CMV-LucF cell line

2000 cells suspended in 200 μL medium were seeded in 16-well plates for 48 h before being transferred into media that contained or without nanoparticles. The iron concentration for both MNCs and DOX–MNCs was reduced to 0.5 mg mL^{-1} but the DOX concentration was the same as in the previous internalizing RM1 cell line hyperthermia protocol. The cells of positive groups were treated 30 min under the AMF (f = 217 kHz) at either 42 °C or 43 °C. The temperature was adjusted by tuning the field amplitude H of the AMF. After that, the following steps were the same as mentioned before.

Statistical analysis

In order to acquire significant results, all experiments were accomplished in triplicate. Statistical analysis was performed using the Student's t-test for unpaired data and the results are presented as mean ± standard deviations. Statistical significance was accepted at a level of $p < 0.05$.

Conclusions

In our previous paper, the excellent chemical and physical performances of a successfully constructed dual response drug nanocarrier have already been demonstrated but only *ex vitro* and without AMF application. Therefore, this comprehensive biological study further establishes the biocompatibility and the therapeutic efficiency of our system under an applied AFM *in vitro*, which will guide the further translation steps into medical application, first through preclinical assays on animals. The MNCs used were found to be biocompatible and efficient as nanoheaters even for concentrations as low as 1 mg mL^{-1}. A significant variation of MNC cellular uptake between different cell lines has been demonstrated *via* multiple techniques. Besides, the previous publication prediction was based on the *ex vitro* simulative drug release profiles only. Here the DOX–MNCs have been revealed to be taken up through endocytosis and to capture a considerable DOX amount within the cytoplasm, without further macroscopic heating stimulation, which results in slow DOX delivery to the nuclei. This affected both the DOX–MNC induced cytotoxicity and the combination therapy effects for these cell lines. More specifically, this dual response system limited the cellular and systemic cytotoxicity compared to free DOX without AMF stimulation, enabling the lower side-effect when the therapy is applied *in vivo*. The thermo–chemotherapy treatment implemented with our system presented a much more potent and synergistic effect than either chemotherapy or magnetic hypothermia alone, for multi-modal cancer therapy in nearly every studied condition. An almost complete cell death was observed for U-87 and MCF-7 cell lines. Moreover, our study demonstrated for the first time a detailed comparison of magnetic nanoparticle stimulated thermo-chemotherapy between intracellular heating and extracellular heating in multiple cell lines. The results indicated that each cell line has different behaviours and responses from one another to the deposited thermal dose and heating application pathway in the combination treatment, which highlights the necessity to study each cell line independently for a given treatment. These promising *in vitro* results confirm that the successful development of DOX-loaded dual pH- and thermo-responsive magnetic nanocarriers constitutes a step forward towards the design of the next generation of nanosystems that are envisioned for future *in vivo* and clinical applications.

Conflicts of interest

There are no conflicts to declare.

Acknowledgements

NTKT thanks EPSRC (EP/M015157/1 and EP/M018016/1); AOARD (FA2386-17-1-4042 award) and European COST action TD1402 RadioMag for funding. AH was supported by the UCL-JAIST PhD program. This study was achieved within the context of the Laboratory of Excellence TRAIL ANR-10-LABX-57. Dr Florian Aubrit is acknowledged for contributing to the drawing of the journal cover artwork.

Notes and references

1 R. D. Issels, *Eur. J. Cancer*, 2008, **44**, 2546–2554.
2 M. W. Dewhirst, B. L. Viglianti, M. Lora-Michiels, M. Hanson and P. J. Hoopes, *Int. J. Hyperthermia*, 2003, **19**, 267–294.
3 P. Prakasa Babu, Y. Yoshida, M. Su, M. Segura, S. Kawamura and N. Yasui, *Neurosci. Lett.*, 2000, **291**, 196–200.
4 J. Yoo, H. R. C. Kim and Y. J. Lee, *Int. J. Hyperthermia*, 2006, **22**, 713–728.
5 P. Clerc, P. Jeanjean, N. Hallalli, M. Gougeon, B. Pipy, J. Carrey, D. Fourmy and V. Gigoux, *J. Controlled Release*, 2018, **270**, 120–134.
6 A. Dieing, O. Ahlers, B. Hildebrandt, T. Kerner, I. Tamm, K. Possinger and P. Wust, *Prog. Brain Res.*, 2007, **162**, 137–152.
7 V. J. Verwaal, S. Bruin, H. Boot, G. Van Slooten and H. Van Tinteren, *Ann. Surg. Oncol.*, 2008, **15**, 2426–2432.
8 D. M. Katschinski, G. J. Wiedemann, W. Longo, F. R. D'Oleire, D. Spriggs and H. I. Robins, *Cytokine Growth Factor Rev.*, 1999, **10**, 93–97.
9 Y. Harima, K. Nagata, K. Harima, V. V. Ostapenko, Y. Tanaka and S. Sawada, *Int. J. Hyperthermia*, 2009, **25**, 338–343.
10 H. I. Robins, J. D. Cohen, C. L. Schmitt, K. D. Tutsch, C. Feierabend, R. Z. Arzoomanian, D. Alberti, F. D'Oleire, W. Longo, C. Heiss, D. Rushing, R. Love and D. Spriggs, *J. Clin. Oncol.*, 1993, **11**, 1787–1794.
11 P. Wust, B. Hildebrandt, G. Sreenivasa, B. Rau, J. Gellermann, H. Riess, R. Felix and P. Schlag, *Lancet Oncol.*, 2002, **3**, 487–497.

12 Z. X. Wang, B. Zhang, S. M. Deng and S. J. Chen, *Chin. Med. J.*, 2012, **125**, 657–661.
13 G. J. Wiedemann, E. Knop, M. Mentzel, J. Geisler, T. Wagner, S. Eleftheriadis, P. Schmucker, M. Klouche, T. Feyerabend, C. Weiss, S. Feddersen, P. Bucsky and F. D'Oleire, *Cancer Res.*, 1994, **54**, 5346–5350.
14 G. Helmlinger, F. Yuan, M. Dellian and R. K. Jain, *Nat. Med.*, 1997, **3**, 177–182.
15 B. Hildebrandt, P. Wust, O. Ahlers, A. Dieing, G. Sreenivasa, T. Kerner, R. Felix and H. Riess, *Crit. Rev. Oncol. Hematol.*, 2002, **43**, 33–56.
16 H. Maeda, J. Wu, T. Sawa, Y. Matsumura and K. Hori, *J. Controlled Release*, 2000, **65**, 271–284.
17 H. Maeda, *J. Controlled Release*, 2012, **164**, 138–144.
18 I. Hilger, *Int. J. Hyperthermia*, 2013, **29**, 828–834.
19 S. T. Heijkoop, H. C. van Doorn, L. J. A. Stalpers, I. A. Boere, J. van der Velden, M. Franckena and A. M. Westermann, *Int. J. Hyperthermia*, 2013, **6736**, 1–5.
20 R. K. Gilchrist, R. Medal, W. D. Shorey, R. C. Hanselman, J. C. Parrott and C. B. Taylor, *Ann. Surg.*, 1957, **146**, 596–606.
21 K. Maier-Hauff, R. Rothe, R. Scholz, U. Gneveckow, P. Wust, B. Thiesen, A. Feussner, A. von Deimling, N. Waldoefner, R. Felix and A. Jordan, *J. Neuro-Oncol.*, 2007, **81**, 53–60.
22 M. Johannsen, U. Gneveckow, K. Taymoorian, B. Thiesen, N. Waldöfner, R. Scholz, K. Jung, A. Jordan, P. Wust and S. A. Loening, *Int. J. Hyperthermia*, 2007, **23**, 315–323.
23 Z. Hedayatnasab, F. Abnisa and W. M. A. W. Daud, *Mater. Des.*, 2017, **123**, 174–196.
24 J. Kolosnjaj-Tabi, R. Di Corato, L. Lartigue, I. Marangon, P. Guardia, A. K. A. Silva, N. Luciani, O. Clément, P. Flaud, J. V. Singh, P. Decuzzi, T. Pellegrino, C. Wilhelm and F. Gazeau, *ACS Nano*, 2014, **8**, 4268–4283.
25 R. T. Gordon, J. R. Hines and D. Gordon, *Med. Hypotheses*, 1979, **5**, 83–102.
26 A. Jordan, R. Scholz, P. Wust, H. Schirra, T. Schiestel, H. Schmidt and R. Felix, *J. Magn. Magn. Mater.*, 1999, **194**, 185–196.
27 A. Jordan, R. Scholz, K. Maier-Hauff, M. Johannsen, P. Wust, J. Nadobny, H. Schirra, H. Schmidt, S. Deger, S. Loening, W. Lanksch and R. Felix, *J. Magn. Magn. Mater.*, 2001, **225**, 118–126.
28 C. Blanco-Andujar, D. Ortega, P. Southern, S. A. Nesbitt and N. T. K. Thanh, *Nanomedicine*, 2016, **11**, 121–136.
29 V. T. A. Nguyen, M. C. De Pauw-Gillet, M. Gauthier and O. Sandre, *Nanomaterials*, 2018, **8**, 1014.
30 P. Moroz, S. K. Jones and B. N. Gray, *Int. J. Hyperthermia*, 2002, **18**, 267–284.
31 Y. Rabin, *Int. J. Hyperthermia*, 2002, **18**, 194–202.
32 A. Hervault, A. E. Dunn, M. Lim, C. Boyer, D. Mott, S. Maenosono and N. T. K. Thanh, *Nanoscale*, 2016, **8**, 12152–12161.
33 S. V. Spirou, S. A. Costa Lima, P. Bouziotis, S. Vranješ-Djurić, E. K. Efthimiadou, A. Laurenzana, A. I. Barbosa, I. Garcia-Alonso, C. Jones, D. Jankovic and O. L. Gobbo, *Nanomaterials*, 2018, **8**, 306.
34 S. Naahidi, M. Jafari, F. Edalat, K. Raymond, A. Khademhosseini and P. Chen, *J. Controlled Release*, 2013, **166**, 182–194.
35 I. Fratoddi, *Nanomaterials*, 2018, **8**, 1–23.
36 X. Li, L. Wang, Y. Fan, Q. Feng and F. Z. Cui, *J. Nanomater.*, 2012, 1–19.
37 R. Gref, A. Domb, P. Quellec, T. Blunkc, R. H. Müllerd, J. M. Verbavatze and R. Langer, *Bone*, 1995, **23**, 1–7.
38 G. Zhang, Z. Yang, W. Lu, R. Zhang, Q. Huang, M. Tian, L. Li, D. Liang and C. Li, *Biomaterials*, 2009, **30**, 1928–1936.
39 D. E. Owens and N. A. Peppas, *Int. J. Pharm.*, 2006, **307**, 93–102.
40 G. Hemery, C. Genevois, F. Couillaud, S. Lacomme, E. Gontier, E. Ibarboure, S. Lecommandoux, E. Garanger and O. Sandre, *Mol. Syst. Des. Eng.*, 2017, **2**, 629–639.
41 J. L. Nitiss, *NIH Public Access*, 2009, **9**, 1–27.
42 C. F. Thorn, C. Oshiro, S. Marsh, T. Hernandez-Boussard, H. McLeod, T. E. Klein and R. B. Altman, *Pharmacogenet. Genomics*, 2011, **21**, 440–446.
43 Z. Zhao, D. Huang, Z. Yin, X. Chi, X. Wang and J. Gao, *J. Mater. Chem.*, 2012, **22**, 15717–15725.
44 K. K. Upadhyay, A. N. Bhatt, A. K. Mishra, B. S. Dwarakanath, S. Jain, C. Schatz, J. F. Le Meins, A. Farooque, G. Chandraiah, A. K. Jain, A. Misra and S. Lecommandoux, *Biomaterials*, 2010, **31**, 2882–2892.
45 O. Taratula, R. K. Dani, C. Schumann, H. Xu, A. Wang, H. Song, P. Dhagat and O. Taratula, *Int. J. Pharm.*, 2013, **458**, 169–180.
46 A. D. Heibein, B. Guo, J. A. Sprowl, D. A. MacLean and A. M. Parissenti, *BMC Cancer*, 2012, **12**, 1–14.
47 J. White, A. Helenius and M. J. Gething, *Nature*, 1982, **300**, 658–659.
48 S. Zhang, H. Gao and G. Bao, *ACS Nano*, 2015, **9**, 8655–8671.
49 G. Sahay, D. Y. Alakhova and A. V. Kabanov, *J. Controlled Release*, 2010, **145**, 182–195.
50 S. Aluri, S. M. Janib and J. A. Mackay, *Adv. Drug Delivery Rev.*, 2009, **61**, 940–952.
51 M. Shi, K. Ho, A. Keating and M. S. Shoichet, *Adv. Funct. Mater.*, 2009, **19**, 1689–1696.
52 A. Hervault and N. T. K. Thanh, *Nanoscale*, 2014, **6**, 11553–11573.
53 K. Fang, L. Song, Z. Gu, F. Yang, Y. Zhang and N. Gu, *Colloids Surf., B*, 2015, **136**, 712–720.
54 M. L. Mojica Pisciotti, E. Lima, M. Vasquez Mansilla, V. E. Tognoli, H. E. Troiani, A. A. Pasa, T. B. Creczynski-Pasa, A. H. Silva, P. Gurman, L. Colombo, G. F. Goya, A. Lamagna and R. D. Zysler, *J. Biomed. Mater. Res., Part B*, 2014, **102**, 860–868.
55 C. Blanco-Andujar, D. Ortega, P. Southern, S. A. Nesbitt, N. T. K. Thanh and Q. A. Pankhurst, *Nanomedicine*, 2016, **11**, 121–136.
56 M. Yonezawa, T. Otsuka, N. Matsui, H. Tsuji, K. H. Kato, A. Moriyama and T. Kato, *Int. J. Cancer*, 1996, **66**, 347–351.
57 F. Valeriote and H. Lin, *Cancer Chemother. Rep.*, 1975, **59**, 895–900.
58 F. Mohamed, P. Marchettini, O. A. Stuart, M. Urano and P. H. Sugarbaker, *Ann. Surg. Oncol.*, 2003, **10**, 463–468.

59 J. P. May and S. D. Li, *Expert Opin. Drug Delivery*, 2013, **10**, 511–527.
60 M. Peller, L. Willerding, S. Limmer, M. Hossann, O. Dietrich, M. Ingrisch, R. Sroka and L. H. Lindner, *J. Controlled Release*, 2016, **237**, 138–146.
61 S. Nagaoka, S. Kawasaki, Y. Karino, Y. Hiraki and T. Nakanishi, *J. Radiat. Res.*, 1987, **28**, 262–267.
62 L. Adumeau, C. Genevois, L. Roudier, C. Schatz, F. Couillaud and S. Mornet, *Biochim. Biophys. Acta, Gen. Subj.*, 2017, **1861**, 1587–1596.
63 A. E. Dunn, D. J. Dunn, A. Macmillan, R. Whan, T. Stait-Gardner, W. S. Price, M. Lim and C. Boyer, *Polym. Chem.*, 2014, **5**, 3311–3315.